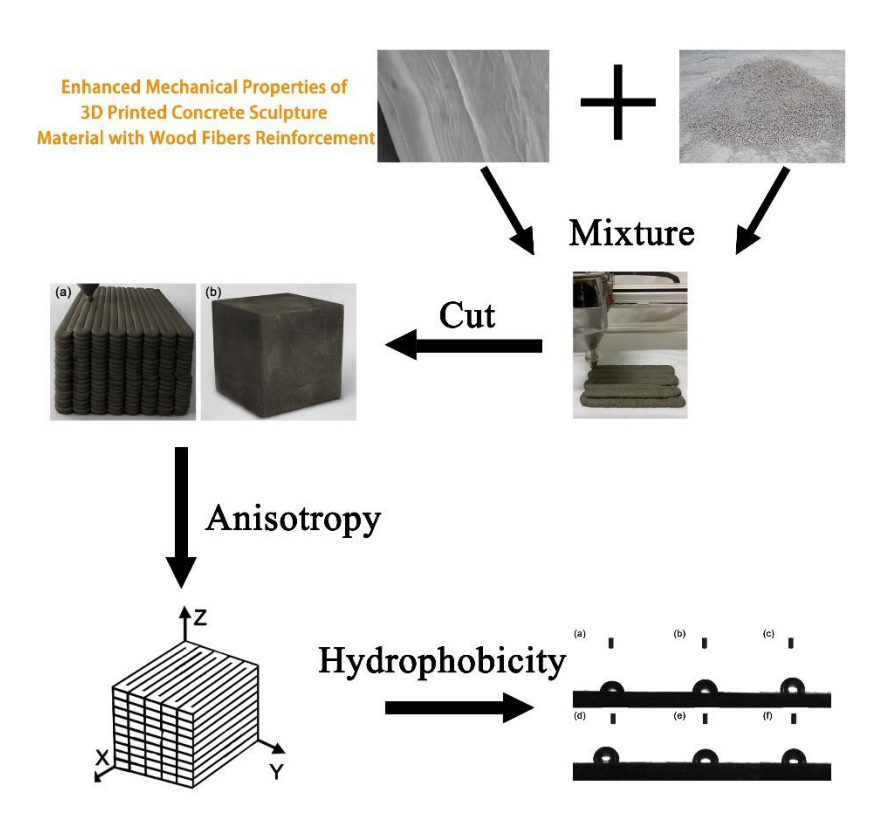
Enhanced Mechanical Properties of 3D Printed Concrete Sculpture Material with Wood Fibers Reinforcement

Kejia Zhang, a,b and Muhammad Fadhil Wong bin Abdullah a,*

* Corresponding author: fadhil.wong@fskik.upsi.edu.my (F.M.)

DOI: 10.15376/biores.19.4.9727-9740

GRAPHICAL ABSTRACT



Enhanced Mechanical Properties of 3D Printed Concrete Sculpture Material with Wood Fibers Reinforcement

Kejia Zhang, a,b and Muhammad Fadhil Wong bin Abdullah a,*

This study examined the mechanical characteristics of 3D printed concrete utilized in sculpture materials, with an emphasis on the incorporation of wood fibers. A series of experiments were conducted to probe into the wood fiber-reinforced 3D printed concrete sculpture materials. Through mechanical and microscopic examinations, the role of flexible fibers in enhancing the bearing capacity of concrete 3D printed components was investigated. The results indicated that an optimal amount of wood fiber addition significantly improved the mechanical properties of the concrete sculpture materials. At the interlayer interface, wood fibers exhibited elongation, thereby mitigating the specimen damage. However, beyond a certain threshold, the mechanical properties tended to decline due to either the agglomeration or direct dislodgment of wood fibers at the interlayer interface, which resulted in an absence of notable deformation. This scenario thereby failed to impede crack propagation. Hydrophobic performance assays revealed an elevation in surface hydrophobicity of 3D printed concrete sculpture materials with the inclusion of wood fibers. Yet, an excessive amount of wood fibers caused a gradual reduction in the contact angle, implying a decrease in the hydrophobicity of the material surface.

DOI: 10.15376/biores.19.4.9727-9740

Keywords: 3D printing technology; Concrete sculptural materials; Fiber reinforcement; Mechanical properties

Contact information: a: Faculty of Art, Sustainability and Creative Industry Universiti Pendidikan Sultan Idris 710105 Malaysia; b: Fine Arts and Art Design College, Qiqihar University, 161000, China; *Corresponding author: fadhil.wong@fskik.upsi.edu.my (F.M.)

INTRODUCTION

The advent of 3D printed concrete materials has brought about a technological shift within the sculpture industry. Concrete 3D printing offers various advantages, including expedited manufacturing, labor reduction, and enhanced safety, garnering extensive attention for its application development. Nonetheless, it presents certain challenges necessitating resolution, such as low bonding strength between layers, insufficient reinforcement, and the requirement for rheological property optimization. Traditional rebar reinforcement methods are incompatible with concrete 3D printing technology, thus paving the way for wood fiber reinforcement as an alternative strategy to augment tensile strength and ductility, to mitigate shrinkage cracking susceptibility, and to boost constructability. Such composites are composed of directional fiber in combination with epoxy resin, which can achieve excellent mechanical properties (Compton and Lewis 2014). A review of pertinent literature revealed substantial scholarly engagement in optimizing the mechanical properties and workability of printable concrete sculpture materials, predominantly *via* wood fiber utilization.

Zhang et al. (2019) and Kruger et al. (2019) posited that the extrusion and stacking processes inherent in 3D printing necessitate high toughness for engineering applications. Wood fiber reinforcement has emerged as a prevalent technique to enhance the ductility and toughness of concrete sculpture materials. Zhu et al. (2021) performed a feasibility study assessing the working performance and mechanical properties of concrete sculpture materials utilizing polypropylene (PP) fibers of 6 mm length with varying added amounts. Liu et al. (2022) acquired printable polyvinyl alcohol (PVOH) fiber-reinforced concrete sculpture materials, which were evaluated with the slump test, permeability test, and printability test. Subsequently, the fiber reinforcement mechanism within fiber concrete sculpture materials was scrutinized via non-destructive ultrasonic pulse test, mechanical property test, and electron microscope scanning test. Sun et al. (2022) employed PVOH fibers to ameliorate the brittle damage mode of cement-based materials, optimizing the mix ratio based on material properties, and investigating the effect of print path on durability alongside defect distribution in printed components through computerized tomography (CT), thereby analyzing the mechanisms influencing durability. Zhang et al. (2022) utilized carbon fibers to formulate printable concrete sculpture composites, where effective impregnation of carbon fibers yielded continuous carbon fiber-reinforced polymer composites with a relatively low void ratio. The excellent fiber-matrix bonding quality made it possible for GF to increase the concrete's strength qualities and reduce water absorption (Ahmad et al. 2022). The study explored the impact of extrusion force on void distribution of 3D printed composites by modulating ply thickness, further optimizing printing process parameters predicated on printing strength. Fang et al. (2018) probed into the compressive, flexural strength, and water resistance of fiber-glass-reinforced magnesium phosphate cement mortar with fiber volume fractions of 1.5, 2.5, 3, and 3.5%. The outcomes showed that an optimal volume fraction of glass fibers at 2.5% manifested a more pronounced effect on flexural strength as compared to compressive strength. Mahmood et al. (2021) considered the influence of fiber reinforcement on the properties of geopolymer concrete composites, noting that fibrous material inclusion transitioned the brittle behavior of concrete alongside significant enhancements in mechanical properties such as toughness, strain, and flexural strength. There have been many quantitative analyses on the material properties of concrete reinforced with wood fiber-based substances through indoor tests (Wang et al. 2019; Wang et al. 2020; Afroughsabet et al. 2015; Bhutta et al. 2017; Fu et al. 2021; Rashid et al. 2020; Wang, J. et al. 2021a; Sun, W et al. 2002; Zhong, H. et al. 2020). The cited research included investigation of the effects of chloride salts, freeze-thaw cycles, and applied loads on concrete properties, illustrating that fibrous substance incorporation could significantly improve the flexural properties, compressive strength, impact properties, splitting tensile strength, durability, and microstructural properties of concrete.

In the present study, 3D printing technology was explored as a burgeoning construction technology that is being used for concrete sculpture material. However, the approach embodies certain drawbacks such as suboptimal molding quality, weak interlayer forces of molded components, and inadequate bearing capacity of molded components in three dimensions, which impede the advancement of concrete 3D printing technology. Consequently, this paper endeavors to spotlight the mechanical properties of concrete 3D printed sculpture materials, probing into potential enhancement methodologies.

EXPERIMENTAL

Materials

The specified amount of residue in the sifted cement was 1.8%. The P•O 42. 5R ordinary silicate cement (Ordinary Portland cement, OPC, 42.5 R, Hua Dye Chemical Co., Ltd., Shanghai, China) had a fineness of 1.8%. The chemical composition of this cement is presented in Table 1. The fumed silica (Hua Dye Chemical Co., Ltd., Shanghai, China) had a SiO₂ content of 94%, and an apparent density of 1649 kg/m³. In the study, poplar wood fiber was used as reinforcement material and the waste was mainly in the form of sawdust.

Table 1. Major Chemical Constituents of Cement (wt%)

Component	CaO	SiO ₂	AL ₂ O ₃	Fe ₂ O ₃	MgO	SO ₃	K ₂ O	TiO ₂
Percentage	69.59	21.61	3.57	2.78	2.21	1.13	0.79	0.32

Poplar residues were extracted using a wood fiber pulverizer (Model 60, Fuyang Energy Technology Co., Ltd., Xuzhou, Jiangsu, China). The poplar microfibers were placed in an impulse-cyclone dryer (Model MQG-50, Jianda Drying Equipment Co., Ltd., Changzhou, China) to prepare well-dispersed poplar fibers. Table 1 lists the fiber morphology of poplar fibers prior to and after drying. The physical index of wood fiber is illustrated in Table 2, and its morphological characteristics are depicted in Fig. 1.

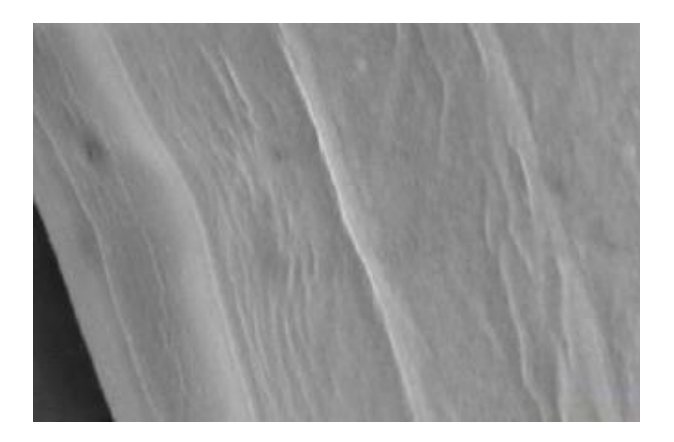


Fig. 1. Wood fiber

Table 2. Performance Indicators of Poplar Fibers Before and After Drying Treatment

Performance Indicator	Before Drying	After Drying
Fiber morphology (mesh)*	60-80	60-80
Fiber length (mm)	1.36(0.20)	1.34(0.11)
Fiber diameter (µm)	223(31)	211(21)
Length-diameter ratio	6.1(1.87)	6.3(0.67)
Moisture content (%)	10.6(0.19)	2.3(0.09)

Note: Particles passed through a 60-mesh screen and were retained on an 80-mesh screen.

Fiber morphology values are usually obtained by microscopic examination. This method enables detailed observation of the diameter, length, shape and surface characteristics of the fiber, thereby quantifying the physical properties of the fiber.

The water repellent agent (P800, Shanghai Kaiin Chemical Co., LTD., Shanghai, China) had the following properties: pH 7 ± 1 ; viscosity, mPa·s 2500 ± 500 (SS-02, 02A type), and storage stability, 12 to 13 months. To clean the fibers, a hydrophobic agent was sprayed onto the surface of the fibers, which were then irradiated with ultraviolet light for 5 to 20 min. The fibers were fumigated in the saturated steam of the hydrophobic agent for 10 to 30 min. The fumigated fibers were removed and sealed. After ultrasonic reaction at 80 to 140 °C for 2 to 3.5 h, they were removed and air dried.

The river sand had a maximum particle size of 2.5 mm (Hua Dye Chemical Co., Ltd., Shanghai, China). Its chemical composition is detailed in Table 3.

Motoriolo	Chemical Composition (%)						
Materials	SiO ₂	CaO	Mgo	AL ₂ O ₃	Fe ₂ O ₃		
Ordinary river sand	68.9	15.7	2.4	9.4	2.7		

Table 3. Chemical Composition of Ordinary River Sand

The water reducing agent (Hua Dye Chemical Co., Ltd., Shanghai, China) was a polycarboxylic acid high-efficiency water reducing agent, exhibiting a water reduction rate of 35% and a solid content of 42%.

Wood fibers were incorporated based on the specified mixing ratios. The length of the wood fibers was 3 mm. The variations in the addition were 0, 0.2, 0.3, 0.4, 0.5, and 0.6%. The detailed proportions of wood fiber are presented in Table 4.

Sample No.	Clinker	Sand	Fly Ash	Silica Fume	Superplasticizer	Retarder	Water	Wood Fibers
1	1	1.09	0.09	0.03	0.04	0.06	0.32	0%
2	1	1.09	0.09	0.03	0.04	0.06	0.32	1%
3	1	1.09	0.09	0.03	0.04	0.06	0.32	2%
4	1	1.09	0.09	0.03	0.04	0.06	0.32	3%
5	1	1.09	0.09	0.03	0.04	0.06	0.32	4%
6	1	1.09	0.09	0.03	0.04	0.06	0.32	5%
7	1	1.09	0.09	0.03	0.04	0.06	0.32	6%

Table 4. Fiber Reinforced Concrete Sculpture Materials with Specified Ratios

Mechanical Sample Preparation and Performance Test

Wood fiber concrete sculpture materials with varying additions were mixed using a concrete mixer (JS1000, Tiande Packaging Machinery Co., Ltd., Weifang, China). The specimens were fabricated *via* Contour Crafting using a 3D building printer (Zhejiang Xunshi Technology Co., Ltd., Shaoxing, China). Optimal results were achieved at a printing speed of 50 mm/s, extrusion speed of 140 mm/s, layer height of 20 mm, and a printer nozzle diameter of 10 mm. The printed cubes had dimensions exceeding 100 mm x 100 mm x 100 mm, as illustrated in Fig. 2(a). Following a 7-day curing period, the specimens were cut into cubes measuring 100 mm×100 mm × 100 mm with a concrete cutter (PLC/Smart-600, Wanlong Times Technology Co., Ltd., Quanzhou, China), as depicted in Fig. 2(b). A microcomputer-controlled cement pressure testing machine

(YAW-S300, Jilin Province Jinli Test Technology Co., Ltd., Changchun, China) was utilized to conduct mechanical tests, as per the GB/T 50081-2002 standard (Cong *et al.* 2019; Singh *et al.* 2019; Song *et al.* 2019; Pan *et al.* 2019). The reported results are the mean values derived from five experimental data points.

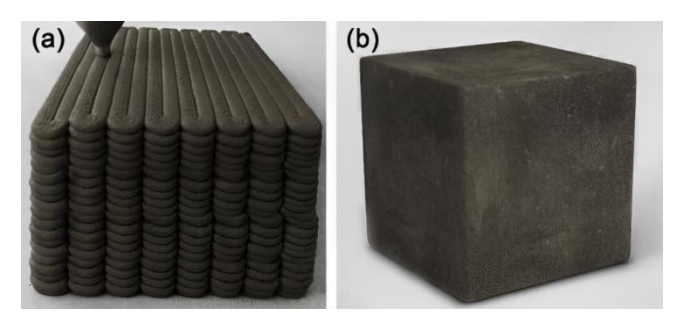


Fig. 2. 3D printed wood fiber concrete sculpture material: (a) printed part (b) cut part

Micromorphological Analysis

For scanning electron microscopy (SEM), the material was fragmented into smaller pieces, and the upward-facing section was flattened. Depending on the purpose of the study, a representative area was selected for cutting to ensure that the sample reflected the overall properties of the material. According to SEM requirements, the sample was cut to the appropriate size, usually between 1 and 3 cm. The sample was positioned in a holder, and a conductive carbon adhesive was applied to both sides. A gold film was evaporated and plated using a vacuum coating process. The morphology and characteristics were observed using a scanning electron microscope (FEI QUANTA200, FEI Company, Netherlands) at an accelerated voltage of 15 kV (Li *et al.* 2022, 2023).

Surface Tension Test

A surface tension meter was employed to measure the contact angle of a specimen at a room temperature of 25 °C. A droplet of liquid was placed on the horizontal surface of the test piece, forming solid-liquid-vapor interface and solid-liquid interface tangents at the solid-liquid-vapor interface junction. The tangents of its gas-liquid interface and solid-liquid interface encapsulated the liquid phase between them at the defined angle. Upon contact with the pigments, the free energy of the system decreased, allowing the experimental liquid to diffuse automatically on the paint surface and form a specific contact angle with the pigment surface. In a state of equilibrium on the pigment plane, the sum of these interfacial tensions in the horizontal direction equals zero, as described by the Young-Laplace equation,

$$\gamma_{SG} - \gamma_{SL} = \gamma_{LG} \cdot \cos\theta \tag{1}$$

where γ_{SG} is the solid-gas interfacial tension, γ_{LG} is the liquid-gas interfacial tension, and γ_{SL} is the solid-liquid interfacial tension. The angle θ is located at the junction of solid, gas and liquid phases. The angle at which θ passes from the pigment interface through the interior of the experimental liquid reagent to the gas-liquid interface is called the contact angle. The contact angle can have values between 0° and 180° . The contact angle is a reaction to the wettability relationship between the pigments and the experimental liquid reagent. The experimental process is tested according to the "Surface and Interfacial Tension Determination Method" SY/T 5370-1999 national standard (Li *et al.* 2017a,b, 2020).

RESULTS AND DISCUSSION

Anisotropy

The rippled edges and local defects formed during the 3D printing process were observed and showed effects in tests of the material's mechanical properties. In the three-way compression test, the results of crack patterns and strength in different directions showed the anisotropy of the sample. The uneven bonding between the middle layers and the gaps caused by the printing path resulted in uneven stress distribution in different loading directions, which led to different damage modes. The 3D printed wood fiber concrete sculpture material was anisotropic in the spatial X, Y, and Z directions. Its loading direction is shown in Fig. 3.

The construction process of concrete 3D printing exhibited unique characteristics. During the printing process, the specimen edges had a corrugated morphology, and the nozzle walkback resulted in localized defects. A locally heterogeneous sample is one in which physical properties (such as density, strength, and porosity) differ significantly in different regions of the material. This non-uniformity is mainly caused by the 3D printing process, including uneven material deposition, temperature changes, and differences in bond strength between layers. During 3D printing, the speed at which the nozzle moves, the fluidity of the material, and the bonding between layers all affect the uniformity of the final structure. During the curing process, the material may have different degrees of shrinkage in different regions due to uneven cooling, resulting in stress concentration and cracks. The distribution and mixing of wood fibers can be uneven, affecting the bonding between the layers and the overall strength. In a three-way compression test, the 3D printed specimen manifests cracking along the vertical strip, underscoring the anisotropic behavior in the X, Y, and Z dimensions. The genesis of anisotropy can be ascribed to localized unevenness within the specimen and disparate forces culminating in member damage (Wang et al. 2020). The weak interlayer surfaces, coupled with the print path's influence, result in multiple voids within the specimen, leading to stress concentration and subsequent specimen damage. To prepare the specimen for mechanical analysis, a methodical trimming process was employed. The 3D printed specimen was trimmed to yield a cube with dimensions 100 mm x 100 mm x 100 mm, thereby excising the specimen edges and localized defects.

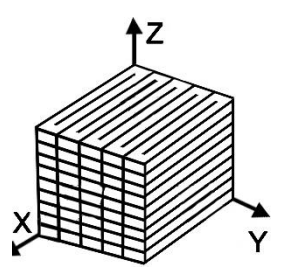


Fig. 3. Schematic of loading direction of 3D typed wood fiber concrete sculpture material

Effect of Wood Fiber on Compressive Strength of Concrete Sculpture Materials

The processed specimens were subjected to mechanical testing using a pressure testing machine; the compressive strengths are shown in Fig. 4. The compressive strength of the material improves with the addition of wood fiber, in the range of 0% to 0.4%. The apex of compressive strength was observed at a 0.4% fiber addition. This value was

attributable to the low modulus of elasticity, large diameter, and effective amalgamation of wood fibers with the concrete sculpture materials. With the addition of wood fiber, the compressive strength of concrete gradually increased in the range of 0% to 0.4%. When the addition of wood fiber reached 0.4%, the compressive strength of concrete reached a peak. This improvement was mainly attributed to the low elastic modulus and large diameter of the wood fiber, which allows it to be effectively integrated into the concrete, improving the toughness and cracking resistance of the overall structure. The tensile strength of wood fiber is a key factor. The tensile strength of wood fibers is a contributing factor. Upon the application of an external force, the fibers deform initially, facilitating partial stress relief. The wood fibers, strategically distributed on the weak interlayer surface, enhance the interlayer bonding, thereby significantly improving the compressive strength of the printed member.

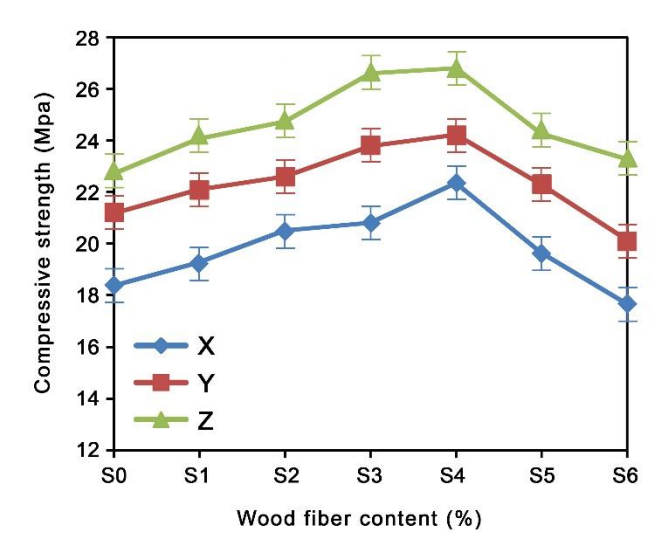


Fig. 4. Compressive strength of wood fiber concrete sculpture material

In the range of 0.5% to 0.6% wood fiber addition, the compressive strength decreased in X, Y, and Z directions. The decrease was obvious in the X direction. The distribution of wood fibers may be uneven, resulting in more defects or voids inside the material, which causes stress concentration. Thus, the compressive strength was significantly reduced. The decrease in the Y direction was relatively mild. In the Y direction, the distribution of wood fibers was more uniform, and the interlayer bonding was better. Therefore, the decrease in compressive strength was small. SEM can directly show the combination of wood fiber and concrete, the propagation path of cracks and the microscopic defects of materials. Thus, it can help account for the change of compressive strength in different directions. Consequently, the interlayer bonding at the weak surface of the layers was diminished. These collective factors contributed to the reduction in compressive strength of the concrete sculpture materials. Therefore, an initial augment followed by a decrement in compressive strength was observed with the increment in wood fiber addition. This is to enhance interlayer bonding, stress dispersion, and toughness. Remarkably, at a 0.4% wood fiber addition, the compressive strength in the Z direction rose to 26.9 MPa, marking the optimum enhancement in mechanical properties. The investigation underscored the pronounced anisotropy in the compressive strength of 3D printed concrete sculpture materials. The superior force direction was identified as the Z direction, followed by the Y direction. A wood fiber addition of 0.4% resulted in an increase in compressive strength across the X, Y, and Z directions. Conversely, a wood fiber addition range of 0.5% to 0.6% led to a decrement in compressive strength across all three directions, with the most significant decrease observed in the X direction.

Effect of Wood Fiber on Splitting Tensile Strength of Concrete Sculpture Materials

The evaluation of splitting tensile strength was conducted on 3D printed concrete specimens with varying additions of wood fibers. Figure 5 encapsulates the results of the investigation. The figure illustrates the variation in splitting tensile strength of 3D printed concrete as influenced by different additions of wood fibers. The splitting tensile strength in both X and Y directions exhibited an initial increase followed by a decline with escalating quantities of wood fiber addition. Conversely, in the Z direction, a consistent upward trend in splitting tensile strength was noted with the augmentation of wood fiber. The wood fiber can disperse the applied stress in the concrete, reducing stress concentration and thus increasing tensile strength, especially in the Z splitting test. Due to the anisotropy caused by the 3D printing process, the performance in the Z direction was more dependent on the reinforcement of the fibers than in the X and Y directions. The apex of splitting tensile strength in the X direction was realized with 0% wood fiber addition, recording a peak value of 2.4 MPa.

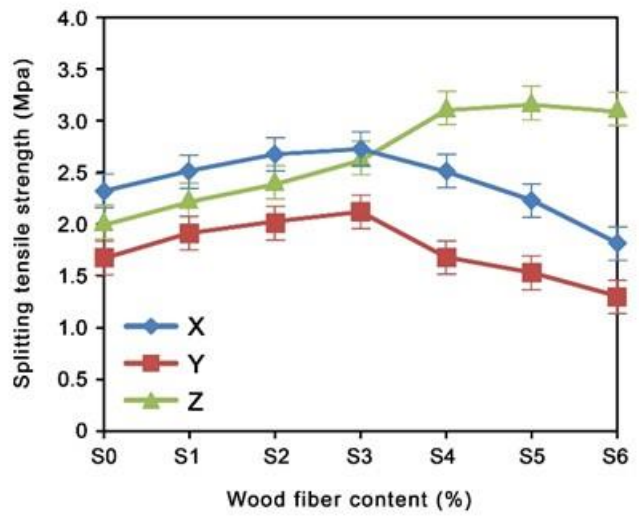


Fig. 5. Effect of wood fiber addition on split tensile strength

On the other end of the spectrum, the Z direction registered the nadir of splitting tensile strength, with a trough value of 2.0 MPa. A comparative analysis with normal concrete revealed that at a 6% wood fiber addition, the splitting tensile strength in the X and Y directions was lower by 21.7% and 23.5% respectively. In stark contrast, the Z direction showcased a robust escalation of 55.0% in splitting tensile strength when juxtaposed with normal concrete.

Effect of Wood Fibers on Flexural Strength of Concrete Sculpture Materials

Figure 6 considers the modulation of flexural strength observed in 3D printed concrete with varying proportions of wood fiber inclusions. The trajectory of flexural strength in the X direction initially rose, then it subsequently fell with increased wood fiber infusion. Conversely, a steady rise in flexural strength was noted in both Y and Z directions.

At a null wood fiber inclusion, the Z direction showed the highest flexural strength, registering a top value of 3.4 MPa, while the X direction showed a trough value of 2.3 MPa. A stark amplification in flexural strength across X, Y, and Z directions by 43.5%, 35.7%, and 41.2% respectively, was observed at a 3% wood fiber infusion, in comparison to normal concrete.

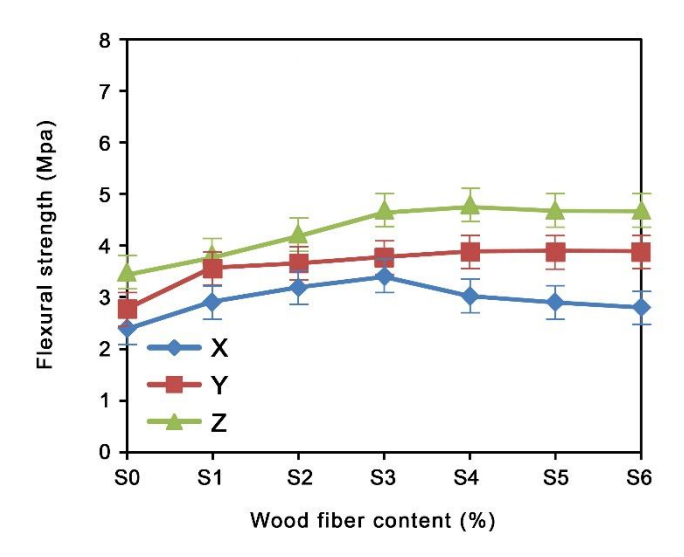


Fig. 6. Effect of wood fiber addition on flexural strength

The degraded bond strength among 3D printed strata appears to play a pivotal role. During the printing process, wood fiber concrete specimens appeared as an array of slender, protracted strips in the horizontal plane. The layer-by-layer printing in the Z direction meant a lesser printing time in the Y-direction, thereby attenuating bond stresses parallel to the X and Y planes. The subsequent rung of bond stresses manifested itself in parallel to the X and Z planes. Upon the exertion of load in the X or Y direction, an expansion perpendicular to the interlayer plane was observed in the wood fiber concrete specimens. However, a Z-direction load induced expansion perpendicular to the plane among adjacent strips. Hence, a diminished compressive strength in the X and Y directions as compared to the Z direction was observed. The splitting tensile strength in the X and Y directions overshadowed that in the Z direction, with the highest point of splitting tensile strength in the Z direction being 3.2 MPa upon escalated wood fiber infusion, surpassing the values in the X and Y directions. The crux of flexural strength was localized at the bottom center of wood fiber concrete specimens, where the tensile stress was highest. The lowest flexural resistance was encountered when loaded in the X direction due to tensile stress acting perpendicular to the adjacent layer exhibiting the feeblest bond strength, resulting in the lowest flexural strength in the X-direction and the highest in the Z direction.

Microscopic Analysis of the Effect of Wood Fibers on the Mechanical Properties of 3D Printed Concrete Specimens

Figure 7 elucidates the interlayer interface dynamics of wood fiber-reinforced concrete sculpture materials, portraying an enhancement in mechanical properties that is attributed to the flexible fibers at these interfaces. In SEM, the material was first cut into small pieces for easy observation. The part facing up was then selected for correction to ensure that the observed interface structure is clear and representative. As delineated in

Fig. 7(d), upon the infliction of pressure-induced damage, the wood fibers at the interlayer interface exhibited elongation, a deformation which in turn dissipated a portion of the energy, thereby mitigating external damage and concurrently retarding the progression of crack development.

A pervasive presence of cracks between adjacent printed layers was noted, undermining the interfacial bonding integrity. After the advent of interlayer interface cracks, the wood fiber located between these cracks was prone to direct pull-out during interlayer slippage, as illustrated in Figs. 7(b) and 7(c). The wood fiber remained relatively undeformed, hence failing to significantly impede the crack propagation. A noteworthy observation was the adhesion of a profusion of hydration products onto the wood fibers traversing through the interlayer interface, which was a consequence of the ongoing cement hydration reaction. The surface of the flexible fiber has a large specific surface area and specific chemical properties, which can effectively adsorb hydration products, such as calcium silicate hydrate (C-S-H). These products are deposited on the fiber surface to form a dense interface. In the process of cement hydration, hydration products accumulate at the interface between fiber and cement matrix, forming enhanced interfacial bond. The release of heat from the hydration reaction and the resulting hydration products promote the reaction process around the fiber. The microstructural visage of these hydration products was predominantly gelatinous. These gels filled the internal structure of the interlayer cracks, reducing the porosity and thereby positively affecting the mechanical properties, as depicted in Fig. 7(e).

With rising proportions of wood fiber inclusion, a fiber agglomeration phenomenon was apparent within the concrete sculpture material, leading to a modification in the internal structure of the specimen and a subsequent augmentation in local porosity. The interlayer bonding at the frail surface interfaces between layers was compromised, as indicated in Fig. 7(f). These intricacies cumulatively precipitated a decline in the compressive strength of the concrete sculpture material. Thus, the increased addition of wood fibers gave a compressive strength trajectory in 3D printed concrete sculpture materials characterized by an initial ascent followed by a descent.

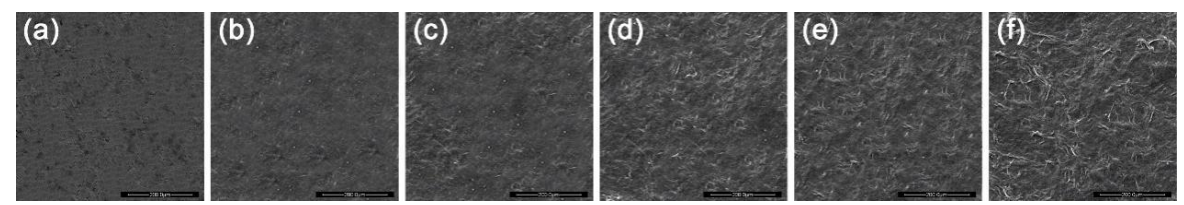


Fig. 7. Scanning electron microscope images of the interlayer interface of wood fiber reinforced concrete sculpture materials

Effect of Wood Fiber on Hydrophobicity of Concrete Sculpture Materials

Inherently, materials such as cement and concrete exhibit hydrophilic tendencies, owing to their molecular structures that have numerous polar groups. They have a pronounced affinity towards water, either attracting water molecules or dissolving therein. The surfaces covered by such molecules are readily wet by water. Some resistance to the initial spreading of water can be attributed to the roughness of the specimen surface. The ingress of air molecules into the fiber network on the specimen surface contributes to surface roughness. In the presence of a sufficient degree of hydrophobic treatment of cellulosic surfaces, such roughness will tend to increase the value of the advancing contact angle of water droplets (Hubbe et al. 2015).

Wood fiber showed strong hydrophobicity after high temperature modification. The addition of wood fibers can effectively enhance the hydrophobicity of concrete sculpture materials. The enhancement of hydrophobicity is shown in the change of contact angle as shown in Fig. 8. The droplets were separately applied to each material (0%, 1%, 2% ... 6% wood fiber) to measure contact angle. The incorporation of wood fibers creates a textured surface morphology that facilitates the trapping of air molecules. This morphology in turn amplifies the surface roughness and further enhances hydrophobicity. Through this mechanism, wood fibers can enhance the hydrophobic properties of concrete sculpture materials, thus providing a practical way to regulate the material's interaction with water.

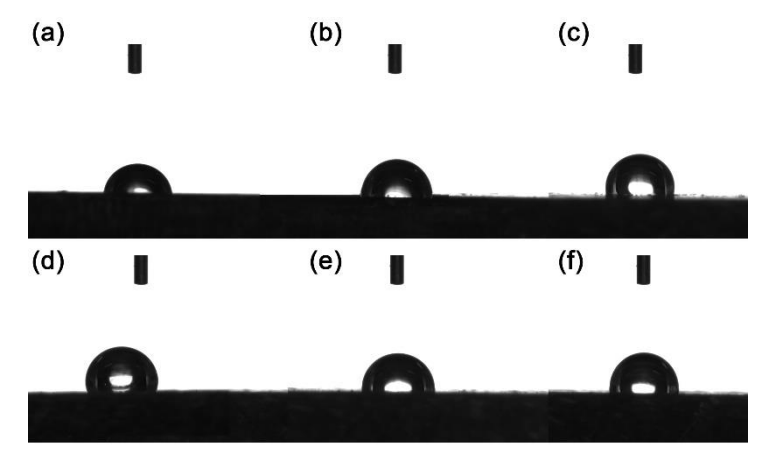


Fig. 8. Change in contact angle(a) Contact angle of newly configured pigment, (b) Contact angle of original pigment

CONCLUSION

- 1. The addition of wood fiber was found to enhance the compressive strength of the concrete sculpture material, peaking at a 0.4% inclusion rate with a compressive strength of 26.9 MPa and a flexural strength of 4.8 MPa. At 0.5% inclusion, the splitting tensile strength reached 3.2 MPa in the Z direction, but compressive strength declined above 0.4% content of wood fiber.
- 2. Microscopic analysis revealed weak bonding at the interlayer interface with microcracks. Elongation of the wood fibers at this interface dissipated energy, delaying crack propagation. These fibers also collect hydration products during cement hydration, partially filling interlayer cracks and enhancing compactness. However, increased wood fiber concentration leads to clumping, raising local porosity and reducing interlayer bonding, ultimately decreasing compressive strength.
- 3. The hydrophobic performance assessment showed that the contact angle of the 3D printed concrete sculpture material increased with wood fiber inclusion, exceeding 90° and indicating enhanced hydrophobicity. However, at wood fiber concentrations of 5 to 6%, the contact angle gradually decreased, suggesting reduced hydrophobicity. This may be due to clustered fibers increasing water permeability, allowing water molecules to access the fiber surface more easily. Additionally, interactions with the cement matrix and hydration products, such as C-S-H gel, can form a film on the fibers, further reducing the contact angle despite the fibers' inherent hydrophobicity.

ACKNOWLEDGEMENTS

Author Contributions

Kejia Zhang and Muhammad Fadhil Wong bin Abdullah conceived of and designed the experiments. Kejia Zhang and Muhammad Fadhil Wong bin Abdullah performed the experiments. Kejia Zhang analyzed and discussed the data. Kejia Zhang wrote the manuscript, with revisions by Muhammad Fadhil Wong bin Abdullah.

Conflicts of Interest

The authors declare no conflict of interest.

REFERENCES CITED

- Afroughsabet, V., and Ozbakkaloglu, T. (2015). "Mechanical and durability properties of high-strength concrete containing steel and polypropylene fibers," *Construction and Building Materials* 94, 73-82. DOI: 10.1016/j.conbuildmat.2015.06.051
- Ahmad, J., González-Lezcano, R. A., Majdi, A., Ben Kahla, N., Deifalla, A. F., and El-Shorbagy, M. A. (2022). "Glass fibers reinforced concrete: Overview on mechanical, durability and microstructure analysis," *Materials* 15(15). DOI: 10.3390/ma15155111
- Bhutta, A., Borges, P. H., Zanotti, C., Farooq, M., and Banthia, N. (2017). "Flexural behavior of geopolymer composites reinforced with steel and polypropylene macro fibers. *Cement and Concrete Composites* 80, 31-40. DOI: 10.1016/j.cemconcomp.2016.11.014
- Compton, B. G., and Lewis, J. A. (2014). "3D-printing of lightweight cellular composites," *Advanced Materials* 26(34), 5930-5935. DOI: 10.1002/adma.201401804
- Cong, L., Jialin, L., Jing, C., Hailun, W., and Dong, L. (2019). "Study on the application of recycled fine powder in ready-mixed concrete," in: *MATEC Web of Conferences*, Vol. 278, p. 01010, EDP Sciences. DOI: 10.1051/matecconf/201927801010
- Fang, Y., Chen, B., and Oderji, S. Y. (2018). "Experimental research on magnesium phosphate cement mortar reinforced by glass fiber," *Construction and Building Materials* 188, 729-736. DOI: 10.1016/j.conbuildmat.2018.08.153
- Fu, Q., Niu, D., Li, D., Wang, Y., Zhang, J., and Huang, D. (2018). "Impact characterization and modelling of basalt–polypropylene fibre-reinforced concrete containing mineral admixtures," *Cement and Concrete Composites* 93, 246-259. DOI: 10.1016/j.cemconcomp.2018.07.019
- GB/T 50081 (2002). "Standard for test methods of physical and mechanical properties of concrete," Standardization Administration of China, Beijing, China.
- Hubbe, M. A., Gardner, D. J., and Shen, W. (2015). "Contact angles and wettability of cellulosic surfaces: A review of proposed mechanisms and test strategies," *BioResources* 10(4), 8657-8749. DOI: 10.15376/biores.10.4.Hubbe_Gardner_Shen
- Kruger, J., Zeranka, S., and van Zijl, G. (2019). "An ab initio approach for thixotropy characterisation of (nanoparticle-infused) 3D printable concrete," *Construction and Building Materials* 224, 372-386. DOI: 10.1016/j.conbuildmat.2019.07.078
- Li, M., and Li, Q. (2022). "Universitas Potensi Utama's curriculum reform for virtual reality education laboratory system," in: *Proceedings of the 5th International*

- Conference on Big Data and Education, pp. 7-14. DOI: 10.1145/3524383.3524411 Association for Computing Machinery, New York, NY, USA, 7-14.
- Li, Q., Chen, F., and Sang, T. (2022). "Effects of wood fiber impulse-cyclone drying process on the UV-accelerated aging properties of wood-plastic composites," PLoS ONE 17(10), article e0266784. DOI: 10.1371/journal.pone.0266784
- Li, Q., Gao, X., Cheng, W., and Han, G. (2017a). "Effect of modified red pottery clay on the moisture absorption behavior and weather ability of polyethylene-based woodplastic composites," Materials 10(111), 2-17. DOI: 10.3390/ma10020111
- Li, Q., Gao, X., Cheng, W., Han, G., and Han, J. (2017b). "Preparation and performance of high-density polyethylene-based wood-plastic composites reinforced with red pottery clay," Journal of Reinforced Plastics and Composites 36(12), 853-863. DOI: 10.1177/0731684417693698
- Li, Q., Liang, Y., Chen, F., and Sang, T. (2020). "Preparation and performance of modified montmorillonite-reinforced wood-based foamed composites," BioResources 15(2), 3566-3584. DOI: 10.15376/biores.15.2.3566-3584
- Li, Q., Sang, T., Li, Y., Li, M., and Sun, Q. (2023). "Intangible cultural heritage complexes in China: Representation and restoration of pigmented reliefs in Kaiping Diaolou," BioResources 18(3), 5665-5682. DOI: 10.15376/biores.18.3.5665-5682
- Liu, B., Liu, X., Li, G., Geng, S., Li, Z., Weng, Y., and Qian, K. (2022). "Study on anisotropy of 3D printing PVA fiber reinforced concrete using destructive and nondestructive testing methods," Case Studies in Construction Materials 17, article e01519. DOI: 10.1016/j.cscm.2022.e01519
- Mahmood, A., Noman, M. T., Pechočiaková, M., Amor, N., Petrů, M., Abdelkader, M., Militký, J., Sozcu, S., and Hassan, S. Z. U. (2021). "Geopolymers and fiberreinforced concrete composites in civil engineering," Polymers 13(13), article 2099. DOI: 10.3390/polym13132099
- Pan, Z., Zhou, J., Jiang, X., Xu, Y., Jin, R., Ma, J., Zhuang, Y., Diao, Z., Zhang, S., Si, Q., and Chen, W. (2019). "Investigating the effects of steel slag powder on the properties of self-compacting concrete with recycled aggregates," Construction and Building Materials 200, 570-577. DOI: 10.1016/j.conbuildmat.2018.12.150
- Rashid, M. U. (2020). "Experimental investigation on durability characteristics of steel and polypropylene fiber reinforced concrete exposed to natural weathering action," Construction and Building Materials 250, article 118910. DOI: 10.1016/j.conbuildmat.2020.118910
- Singh, A., Arora, S., Sharma, V., and Bhardwaj, B. (2019). "Workability retention and strength development of self-compacting recycled aggregate concrete using ultrafine recycled powders and silica fume," Journal of Hazardous Toxic and Radioactive Waste 23(4), article 04019016. DOI: 10.1061/(ASCE)HZ.2153-5515.0000456
- Song, W., Zou, D., Liu, T., Teng, J., and Li, L. (2019). "Effects of recycled CRT glass fine aggregate size and content on mechanical and damping properties of concrete," Construction and Building Materials 202, 332-340. DOI: 10.1016/j.conbuildmat.2019.01.033
- Sun, X., Zhou, J., Wang, Q., Shi, J., and Wang, H. (2022). "PVA fibre reinforced highstrength cementitious composite for 3D printing: Mechanical properties and durability," Additive Manufacturing 49, article 102500. DOI: 10.1016/j.addma.2021.102500
- Sun, W., Mu, R., Luo, X., and Miao, C. (2002). "Effect of chloride salt, freeze-thaw cycling and externally applied load on the performance of the concrete," Cement and

- Concrete Research 32(12), 1859-1864. DOI: 10.1016/S0008-8846(02)00769-X
- Wang, J., Dai, Q., Si, R., and Guo, S. (2019). "Mechanical, durability, and microstructural properties of macro synthetic polypropylene (PP) fiber-reinforced rubber concrete," *Journal of Cleaner Production* 234, 1351-1364. DOI: 10.1016/j.jclepro.2019.06.272
- Wang, J., Dai, Q., Si, R., Ma, Y., and Guo, S. (2020a). "Fresh and mechanical performance and freeze-thaw durability of steel fiber-reinforced rubber self-compacting concrete (SRSCC)," *Journal of Cleaner Production* 277, article 123180. DOI: 10.1016/j.jclepro.2020.123180
- Wang, Y. Z., Wang, Y. B., Zhao, Y. Z., Li, G. Q., Lyu, Y. F., and Li, H. (2020). "Experimental study on ultra-high performance concrete under triaxial compression," *Construction and Building Materials* 263, article 120225.
- Wang, Y., Zhang, S., Niu, D., and Fu, Q. (2022). "Quantitative evaluation of the characteristics of air voids and their relationship with the permeability and salt freeze—thaw resistance of hybrid steel-polypropylene fiber—reinforced concrete composites," *Cement and Concrete Composites* 125, article 104292. DOI: 10.1016/j.cemconcomp.2021.104292
- Zhang, Y., Zhang, Y., She, W., Yang, L., Liu, G., and Yang, Y. (2019). "Rheological and harden properties of the high-thixotropy 3D printing concrete," *Construction and Building Materials* 201, 278-285. DOI: 10.1016/j.conbuildmat.2018.12.061
- Zhang, Z., Long, Y., Yang, Z., Fu, K., and Li, Y. (2022). "An investigation into printing pressure of 3D printed continuous carbon fiber reinforced composites," *Composites Part A: Applied Science and Manufacturing* 162, article 107162. DOI: 10.1016/j.compositesa.2022.107162
- Zhong, H., and Zhang, M. (2020). "Experimental study on engineering properties of concrete reinforced with hybrid recycled tyre steel and polypropylene fibres," *Journal of Cleaner Production* 259, article 120914. DOI: 10.1016/j.jclepro.2020.120914
- Zhu, B., Nematollahi, B., Pan, J., Zhang, Y., Zhou, Z., and Zhang, Y. (2021). "3D concrete printing of permanent formwork for concrete column construction," *Cement and Concrete Composites* 121, article 104039. DOI: 10.1016/j.cemconcomp.2021.104039

Article submitted: January 30, 2024; Peer review completed: May 25, 2024; Revised version received: September 25, 2024; Accepted: September 29, 2024; Published: October 30, 2024.

DOI: 10.15376/biores.19.4.9727-9740